

The efficiency of the spiral-in of a black hole to the Galactic centre

Piero F. Spinnato^{a,*}, Michael Fellhauer^b and Simon F. Portegies Zwart^{a,c}

^a*Section Computational Science, Universiteit van Amsterdam, Kruislaan 403, 1098 SJ Amsterdam, The Netherlands*

^b*Institut für Theoretische Physik und Astrophysik der Christian-Albrechts-Universität zu Kiel, Leibnizstr. 15, D-24118 Kiel, Germany*

^c*Astronomical Institute ‘Anton Pannekoek’, Universiteit van Amsterdam, Kruislaan 403, 1098 SJ Amsterdam, The Netherlands*

ABSTRACT

We study the efficiency at which a black hole or dense star cluster spirals-in to the Galactic centre. This process takes place on a dynamical friction time scale, which depends on the value of the Coulomb logarithm ($\ln \Lambda$). We determine the accurate value of this parameter using the direct N -body method, a tree algorithm and a particle-mesh technique with up to 2 million plus one particles. The three different techniques are in excellent agreement. Our measure for the Coulomb logarithm appears to be independent of the number of particles. We conclude that $\ln \Lambda = 6.6 \pm 0.6$ for a massive point particle in the inner few parsec of the Galactic bulge. For an extended object, like a dense star cluster, $\ln \Lambda$ is smaller, with a value of the logarithm argument Λ inversely proportional to the object size.

Key words: methods: N-body simulations – methods: numerical – celestial mechanics, stellar dynamics – black hole physics – Galaxy: bulge.

1 INTRODUCTION

The very young objects near the Galactic centre, such as the Quintuplet star cluster (Nagata et al. 1990; Okuda et al. 1990), the Arches cluster (Nagata et al. 1995) and the central star cluster (Tamblyn & Rieke 1993; Krabbe et al. 1995) are of considerable interest. One of the more interesting conundrums is the presence of stars as young as few Myr (Tamblyn & Rieke 1993; Krabbe et al. 1995) within a parsec from the Galactic centre (Gerhard 2001). *In situ* formation is problematic, due to the strong tidal field of the Galaxy, which makes this region inhospitable for star formation. One possible solution is provided by Gerhard (2001), who proposes that a $10^6 M_{\odot}$ star cluster spirals in to the Galactic centre within a few million years from a distance $\gtrsim 30$ pc. The infall process is driven by dynamical friction (Chandrasekhar 1943). A quantitative analysis of this model by McMillan & Portegies Zwart (2002) confirms Gerhard’s results. The main uncertainty in the efficiency of dynamical friction, and therewith the time scale for spiral-in, is hidden in a single parameter, called the Coulomb logarithm $\ln \Lambda$. Accurate determination of this parameter is crucial for understanding this process. Nevertheless, a precise value of $\ln \Lambda$ for the Galactic central region is not available. In this paper we determine $\ln \Lambda$ for the Galactic centre. We focus on the efficiency of the interaction between an intermediate mass black hole (BH hereafter) and the stars in the Galactic central region. In Section 4 we comment on how this approach can be applied to star clusters that sink to the Galactic centre.

In the classical study of Chandrasekhar (1943), dynamical

friction is driven by the negative drag force experienced by a massive dimensionless body moving through an infinite medium of homogeneous density. The consequences of finiteness and non-homogeneity have been analysed in various works (see Maoz 1993; Milosavljević & Merritt 2001). Still, the original expression of Chandrasekhar remains a valid approximation for dynamical friction in many astronomical situations (see Binney & Tremaine 1987, Section 7.1).

Dynamical friction is important for a large variety of astronomical phenomena, e.g. planet migration (Goldreich & Tremaine 1980; Cionco & Brunini 2002), core collapse in dense star clusters (Portegies Zwart et al. 1999) or mergers in galaxy clusters (Makino 1997; Cora et al. 1997; van den Bosch et al. 1999). The physics of the infall process of a satellite in the parent galaxy is basically the same as in the case of a BH spiralling-in to the Galactic centre. The relevant parameters, however, are quite different in the two cases. For example, an inspiraling galaxy has finite size, whereas a BH is a point mass. Dynamical friction also plays an important role in the evolution of the black hole binary formed after the merging of two galaxies both hosting a BH at their centre (Milosavljević & Merritt 2001). In this case, dynamical friction is important in the early phase of galaxy merging, when the BHs orbits converge and become bound.

We determine the value of $\ln \Lambda$ for a BH spiralling-in to the Galactic centre by means of self-consistent N -body simulations. This is by far not an easy task. N -body models either lack in the number of particles (a direct N -body code can treat up to about 10^5 particles, compared to 10^8 for the real system) or have to introduce softening (Aarseth 1963) and approximation of the force calculation (treecode (Barnes & Hut 1986) or particle-mesh code (Hockney & Eastwood 1988)). The softening parameter ϵ was introduced

* E-mail: piero@science.uva.nl (PS); mike@astrophysik.uni-kiel.de (MF); spz@science.uva.nl (SPZ)

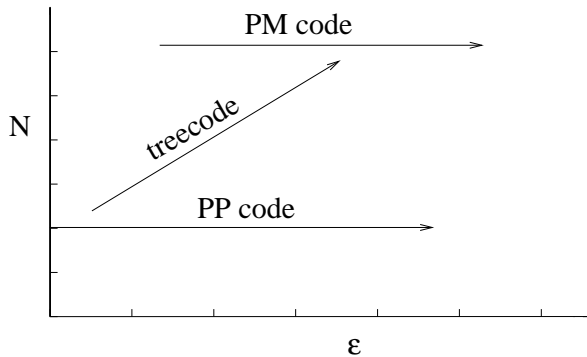


Figure 1. A sketch of the strategy that we adopt in order to explore the ϵ - N parameter space.

to limit the strength of the mutual gravitational interaction during close stellar encounters. Without softening, the very high accelerations experienced by the encountering bodies would cause very tiny integration steps, which would result in a substantial freeze of the global system evolution, with consequent dramatic performance deprivation. The use of such approximation does not corrupt the correctness of the numerical results, as long as the simulated system is studied on a time scale shorter than the relaxation time scale (Binney & Tremaine 1987, ch.4, see also discussion in Section 3.3 below). The dynamical friction time scale of the systems we simulate is in all cases shorter than the relaxation time scale, so we can safely use the approximate methods.

Nevertheless, since close encounters have a relevant effect on dynamical friction, decreasing their strength by means of softening also decreases the strength of dynamical friction, i.e. lowers the value of $\ln \Lambda$. The same role of softening is played, in the particle-mesh code, by the grid cell size l .

Our methodological approach for the present work (see Fig. 1) consists in comparing the “exact” results obtained with the direct method for low particle numbers (up to 80 000) with the results of the treecode, which are less accurate and influenced by force softening, to understand how the softening ϵ influences the results and how they have to be scaled according to the value of ϵ . Then the results of the treecode are compared to the results of the particle-mesh code, to see how softening (tree) and grid-resolution l (particle-mesh) can be compared and scaled. Finally, having the right scaling between the different codes, we will be able to perform high particle number simulations (up to $4 \cdot 10^7$) with the particle-mesh code to obtain the value of the Coulomb logarithm for the inner Galactic Bulge.

2 METHODS AND MODEL

2.1 Direct method

For our direct N -body calculations we used the *kira* integrator module of the Starlab software environment¹ (Portegies Zwart et al. 2001). Conceived and written as an independent alternative to Aarseth’s NBODY4 and NBODY5 (Aarseth 1985, 1999),

the workhorses of collisional N -body calculations for the past 25 years, *kira* is a high-order predictor-corrector scheme designed for simulations of collisional stellar systems. This integrator incorporates a Hermite integration scheme (Makino & Aarseth 1992) and a block time step scheduler (McMillan 1986) that allows homogeneous treatment of all objects in the system.

While *kira* is designed to operate efficiently on general-purpose computers, it achieves by far its greatest speed when combined with GRAPE-6 special purpose hardware (Makino et al. 2002)². For the work presented here we performed simulations with the GRAPE-6 system at the University of Tokyo with up to 80 000 particles.

2.2 Treecode

The hierarchical treecode (Barnes & Hut 1986) is widely used for the simulation of collisionless systems. The force on a given particle i is computed by considering particle groups of larger and larger size as their distance from i increases. Force contributions from such groups are evaluated by using truncated multipole expansions. The grouping is based on a hierarchical tree data structure. Such hierarchical tree is realised by inserting the particles one by one into the initially empty simulation cube. Each time two particles are into the same cube, this is divided into eight ‘child’ cubes, whose linear size is one half of its parent’s. This procedure is repeated until each particle finds itself into a different cube. Hierarchically connecting such cubic cells according to their parental relation leads to the hierarchical tree data structure. When force on particle i is computed, the tree is traversed looking for cells that satisfy an appropriate acceptance criterion; if the cell is not accepted, then its children are checked. See Salmon & Warren (1994) for a detailed overview on acceptance criteria. By applying this procedure recursively starting from the tree root, i.e. the cell containing the whole system, all the cells satisfying the acceptance criterion are found.

Our treecode simulations were initially performed with both a code written by Jun Makino (Makino 1991), and with GADGET (Springel et al. 2001). In GADGET each particle is assigned an individual time-step, and at each iteration only those particles having an update time below a certain time are selected for force evaluation. This criterion was originally introduced in the direct N -body code (*cf.* Aarseth 1999). This code is parallelized using MPI (Message Passing Interface Forum 1997). In the parallel version, the geometrical domain is partitioned, and each processor hosts the particles located in the domain partition assigned to it. The computation of forces on the selected i -particles is performed by scattering the particle data to remote processors. Then partial forces from the particles hosted by the remote processors are computed locally. Finally, calculated forces are received back by the i -particle host, and added up resulting in the total force on the i -particles.

Our tests revealed that GADGET was considerably faster (in part because we run the code on up to 128 processors) and more accurate than Makino’s treecode, because of the use of individual time steps.

2.3 Particle-mesh code

To perform calculations using several millions of particles we use a particle-mesh (PM) code named SUPERBOX (Fellhauer et al.

¹ See: <http://manybody.org>

² See: <http://www.astrogrape.org>

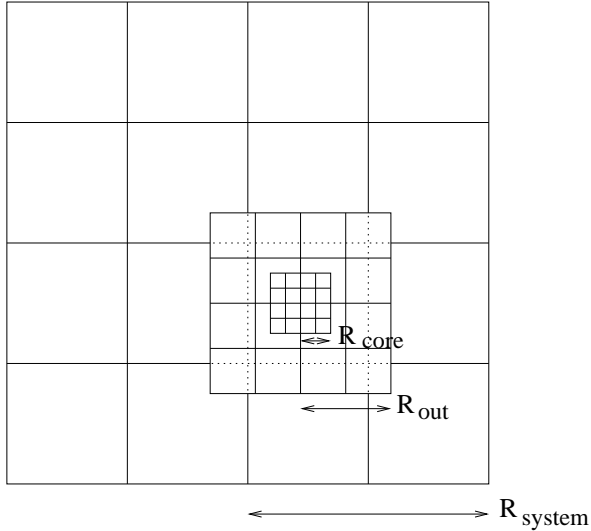


Figure 2. The different grids of SUPERBOX for a number of cells per dimension $n = 4$. The finest and intermediate grids are focussed on the object of interest. Each grid is surrounded by a layer of two halo cells. Such haloes are not shown here.

2000). With the particle-mesh technique densities are derived on Cartesian grids. Using a fast Fourier transform algorithm these densities are converted into a grid-based potential. Forces acting on the particles are calculated using these grid-based potentials, making the code nearly collisionless. The current implementation completely neglects two-body relaxation causing it to retain only a small amount of grid-based relaxation (Fellhauer et al. 2000).

The adopted implementation incorporates some differences to standard PM-codes. State of the art PM-codes are using a cloud-in-cell (CIC) scheme to assign the masses of the particles to the grid-cells; which means that the mass of a particle i is split up into neighbouring cells according to its distance to the centre of the cell. Forces are then calculated by adding up the same fractions of the forces from all cells to particle i . In contrast our code uses the “old-fashioned” nearest-grid-point scheme, where the total mass of the particle is assigned to the grid-cell the particle is located in. Forces acting on the particle are then calculated only from the forces acting on this particular cell. To achieve similar precision as CIC, we use space derivatives up to the second order.

To achieve high resolution at the places of interest, we incorporate for every simulated object (e.g. each galaxy and/or star cluster or disc, bulge and halo) two levels of sub-grids which stay focused on the objects of interest while they are moving through the simulated area (see Fig. 2). This provides higher resolution only where it is necessary. Our PM-code is parallelized using MPI.

2.4 The theory of the Coulomb logarithm

Dynamical friction affects a mass moving in a background sea of lower mass objects. A practical expression for the strength of the drag force on a point particle with mass M_{BH} is (Binney & Tremaine 1987, p. 424):

$$\frac{d\mathbf{v}_{BH}}{dt} = -4\pi G^2 \ln \Lambda \rho M_{BH} \frac{\mathbf{v}_{BH}}{v_{BH}^3} \left[\text{erf}(X) - \frac{2X}{\sqrt{\pi}} e^{-X^2} \right]. \quad (1)$$

Here $X = v_{BH}/(\sqrt{2}\sigma)$, σ being the Maxwellian velocity dispersion, and ρ is the background stellar density.

The classical value of Λ is (Binney & Tremaine 1987, p. 423)

$$\Lambda = \frac{b_{max} v_{typ}^2}{G(M_{BH} + m)}. \quad (2)$$

Here b_{max} is the largest possible impact parameter for an encounter between the massive point particle and a member of the background population, v_{typ} is the typical speed of the objects in the background population, and m is the mass of each of the background stars. Equation (2) can then be generalised to

$$\Lambda = \frac{b_{max}}{b_{min}}. \quad (3)$$

Here b_{min} is the distance below which an encountering particle is captured, instead of being scattered by the massive object. It is somewhat smaller than the 90° turn-around distance. With the direct N -body technique, Λ can be measured precisely. However, with approximate N -body methods, such as the treecode or the PM code, we have to take care of the interference of the softening length/cell size with b_{min} , as discussed in Section 2.5.

McMillan & Portegies Zwart (2002) obtained an analytic expression for the distance $r(t)$ of the BH to the Galactic centre, with the assumptions that the BH’s orbits are nearly circular, and the mass profile of the Galaxy is given by a power law:

$$M(R) = AR^\alpha. \quad (4)$$

They obtained:

$$r(t) = R_0 \left[1 - \frac{\alpha(\alpha + 3)}{\alpha + 1} \sqrt{\frac{G}{AR_0^{\alpha+3}}} \chi M_{BH} \ln \Lambda t \right]^{\frac{2}{3+\alpha}}, \quad (5)$$

where

$$\chi = \text{erf}(X) - \frac{2X}{\sqrt{\pi}} e^{-X^2} \quad \text{and} \quad X = \frac{v_{BH}}{\sqrt{2}\sigma},$$

σ being the velocity dispersion. In McMillan & Portegies Zwart (2002) the value of X in the Galactic centre is also computed, resulting in $X = \sqrt{2 - \alpha}$. Finally, we take R_0 equal to the half-mass radius R_{hm} (see Section 2.6). The best fit of equation (5) on the simulation data gives the value of $\ln \Lambda$ for that simulation. Such values, for all simulation performed, are reported in the last column of Tables 3, 4 and 5.

2.5 The role of softening in the determination of the Coulomb logarithm

As already mentioned in the introduction, softening was introduced in numerical stellar dynamics to limit the strength of mutual forces during close stellar encounters, mainly for computational performance purposes. It consists in a modification of the Newton law for the gravity exerted by a particle j on a particle i , as follows:

$$\mathbf{a}_i = G \frac{m_j}{(r_{ij}^2 + \epsilon^2)^{(3/2)}} \mathbf{r}_{ij} \quad (6)$$

where $\mathbf{r}_{ij} = \mathbf{r}_j - \mathbf{r}_i$, and ϵ is the softening parameter. As $\mathbf{r}_{ij} \rightarrow 0$, the presence of ϵ causes the force to change from inverse square to elastic, with constant $Gm_i m_j / \epsilon^3$. In this way the strength of the mutual force between encountering particles is no more unbound.

Softening was first used by Aarseth (1963) in a particle-particle (PP) context. Accuracy requirements soon led to a more precise treatment of close encounters and binaries by means of an analytic approach (Kustaanheimo & Stiefel 1965; Aarseth 1972;

Mikkola & Aarseth 1990). The softened force in equation (6) remains used in the treecode, where high accuracy in close encounters treatment is not mandatory. Here we will use the softening both in the treecode simulations, where it is necessary, and in the PP code simulations, where it is used to compare the results of the two codes, in order to study the relation between ϵ and $\ln \Lambda$.

For the PM code, as described in Section 2.3, force is not computed by using the Newton force, or the softened force in equation (6). Instead, the fact that the gravitational potential on each grid point of the mesh is obtained from a density field defined on the same mesh, leads to an accuracy for the force on each particle limited by the cell size of the grid, l .

Here, we are concerned with the accuracy of the computation of the encounters experienced by a black hole spiralling-in to the Galactic centre. Since the softening (PP and treecode) and the cell size (PM code) affect this accuracy, we will use ϵ and l to quantify the accuracy decrement in our simulations. In Section 3.4 we will study quantitatively the dependence of $\ln \Lambda$ on ϵ and l .

The reference value for ϵ in the work presented here will be $\epsilon_0 = 0.003735$ (units given below in Table 1). This value, according to Athanassoula et al. (2000), is of the same order of magnitude as the optimal softening for a Dehnen sphere distribution. This distribution is similar to the power law distribution that we use, at least for what concerns the high central density peak, which is the key physical factor in the determination of the optimal softening. For an 80 000 particle distribution, ϵ_0 is about 15 times smaller than the mean inter-particle distance ℓ at the initial BH position $R_0 \simeq 0.87$ (see Section 2.6). This value for ϵ is small enough to avoid spurious effects in the force between a star and its neighbours, but is sufficient to inhibit very close encounters. The expression for ℓ can be obtained as:

$$\ell = n^{-\frac{1}{3}} = \left(\frac{\rho}{m}\right)^{-\frac{1}{3}} = \sqrt[3]{\frac{4\pi R^{3-\alpha}}{NA\alpha}} \quad (7)$$

where n is the star number density, and

$$\rho = \frac{1}{4\pi R^2} \frac{dM}{dR} = \frac{A\alpha}{4\pi} R^{\alpha-3}.$$

We used the expression in equation (4) for M , and the fact that the N stars in the system have the same mass $m = 1/N$.

One of the effects of softening is a dumping in the BH infall at very small values of the galactocentric distance, more noticeable as N increases. This can be explained with the fact that the inter-particle distance ℓ decreases as the BH approaches the Galactic centre (see equation 7). When ℓ becomes comparable to 2ϵ , the role of softening in the force equation becomes dominant, since particles begin to ‘overlap’. With $N = 400\,000$, we get $\ell = 2\epsilon_0$ when $R \simeq 0.064$, which is close to the value at which the dumping arises, as Fig. 12 below clearly shows.

2.6 Initial condition

We generate the initial mass distribution according to the power law given by equation (4), with $\alpha = 1.2$, which reproduces the mass distribution in the centre of the Galaxy, according to Mezger et al. (1999). The scale factor is $A = 4.25 \cdot 10^6 M_\odot$, corresponding to 0.44 in the N -body standard units (Heggie & Mathieu 1985), which are reported in Table 1. We use the standard units hereafter, unless other units are explicitly reported. The distributions that we generate are truncated at $R = 1.7 = 13.6$ pc, with a total mass within this radius $M_{tot} = 1$. The particles have equal mass m . Particles are assigned Maxwellian velocities, then the system is virialised to

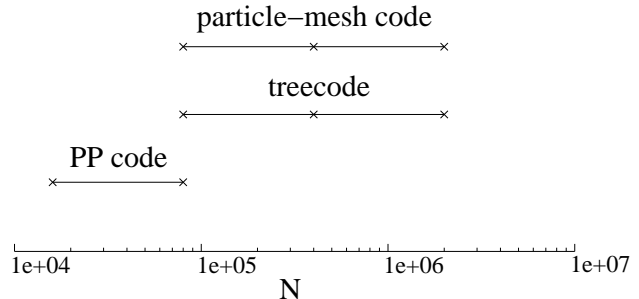


Figure 3. Particle ranges for the simulations performed by each method. Crosses denote the particle values used.

dynamical equilibrium. Then, before inserting the black hole (BH) particle, we let the system evolve for a few crossing times. The system reaches a stable configuration, whose mass profile is no more perfectly reproduced by Eq. 4. The best fit for A and α on the mass profile of the stable configuration gives:

$$\begin{aligned} A &= 0.53 \\ \alpha &= 0.9. \end{aligned} \quad (8)$$

In fact, the mass profile having these coefficients diverges from the original one as the distance R increases. On the other hand, in the region $R < 2$, where we study the BH infall, the discrepancy between the two mass profiles is small. The relaxed profile values are within 10% of the initial profile values. Nevertheless, for consistency we will use the values in equation (8) for A and α hereafter. This results in values of $\ln \Lambda \simeq 10\%$ smaller than the ones given by a mass profile with coefficients $\alpha = 1.2$ and $A = 0.44$.

The BH particle is placed at the half-mass radius $R_{hm} \simeq 0.87$ with a circular orbit velocity, and its mass is $M_{BH} = 0.000528$. The background particles number varies from 16 000 to 2 million. The low particle number simulations are performed with the PP code, the intermediate and high number simulations with the treecode and the PM code. Fig. 3 shows the particle range for each code. This allows us to span a large range in particle number, so that the influence of granularity in the BH motion towards the Galaxy centre can be studied.

In contrast to the other models, we choose physical units for the PM code simulations. The conversion factors from physical units to N -body units are shown in Table 1, where l.u. denotes the unit length in N -body units, m.u. the unit mass, v.u. the unit velocity and t.u. the unit time.

The parameters of the PM calculations are chosen in the following way: the grid sizes are kept constant at

$$\begin{aligned} R_{\text{system}} &= 140.0 \text{ pc} \\ R_{\text{out}} &= 9.6 \text{ pc} \\ R_{\text{core}} &= 2.4 \text{ pc} \end{aligned} \quad (9)$$

and are focussed on the center of mass of the ‘bulge’ model, as sketched in Fig. 2. To change the resolution we alter the number of grid cells per dimension from 32 up to 128. With this choice the cell sizes listed in Table 2 are achieved.

To avoid a self-acceleration of the black hole we choose $H_{0,0,0} = 1.0$ of the Greens-function, which worsens the energy conservation of the code (see Fellhauer et al. 2000) especially in simulations with high particle numbers per grid cell, but suppresses

Table 1. Conversion table between the N -body units used in our work, and physical units. The N -body units are such that $G = 1$, $M_{tot} = 1$, and $E_{tot} = -0.25$.

$$\begin{aligned}
 G &= 1 \text{ v.u.}^2 \text{ l.u.} / \text{m.u.} \\
 &\equiv 4.3007 \cdot 10^{-3} \text{ km}^2 \text{ pc} / \text{s}^2 \text{ M}_{\odot} \\
 &\equiv 4.49842 \cdot 10^{-3} \text{ pc}^3 / \text{Myr}^2 \text{ M}_{\odot} \\
 1 \text{ l.u.} &= 8 \text{ pc} \\
 1 \text{ m.u.} &= 1.18 \cdot 10^8 \text{ M}_{\odot} \\
 1 \text{ v.u.} &= \sqrt{\frac{G \cdot 1 \text{ m.u.}}{1 \text{ l.u.}}} = 251.86 \text{ km/s} \\
 1 \text{ t.u.} &= \sqrt{\frac{1 \text{ l.u.}^3}{G \cdot 1 \text{ m.u.}}} = 0.031 \text{ Myr}
 \end{aligned}$$

Table 2. Resolutions (i.e. cell sizes) of the different grid levels for the different choices of n in the PM code. n denotes the number of cells per dimension. The cell sizes of the different grid-levels (outer, middle and inner) are given in pc.

n	outer	middle	inner
32	10.00	0.69	0.17
64	4.67	0.32	0.08
128	2.26	0.15	0.04

the forces of particles in the same cell on each other and on themselves.

To speed up the simulations, the time step in the PM code simulations should be as large as possible, but small enough to prevent spurious results. Therefore we started with a time step of 1,000 yr and reduced it to 200 and 50 yr. The results of the 200 yr and 50 yr time step do not differ from each other, therefore the global time step is chosen to be 200 yr. Conversely, the time step in the treecode and direct code simulations is variable and different for each particle. Time step values are in this case in the range 2–30 000 yr, with about 90% of them in the range 100–300 yr.

3 RESULTS

We will now study the dependence of our results on the number of particles N in Section 3.1, and compare the various N -body methods with identical initial realisations in Section 3.2. After having convinced ourselves that the various techniques produce consistent results, we continue by studying the effect of softening/cell size (Section 3.3) and black hole mass (Section 3.5) on the value of the Coulomb logarithm in the inner part of the Galaxy.

Our simulations aimed at several goals. 1) understanding the scaling of the system dynamics with respect to the number of particles N , and within this scaling, how results from different methods compare with each other. 2) How, at a fixed value of N , the softening parameter influences the dynamics, changing the value of $\ln \Lambda$. The particle-mesh method does not make use of softening. The cell size in the PM code can be seen in this context as a softening length. In our framework, it is crucial to understand the relation between the PP code and treecode softening parameter and the PM code cell size. 3) We also study how the BH mass influences the infall time. We doubled and quadrupled the BH mass, and observed how this affects the value of $\ln \Lambda$.

Table 3. Overview of the PP runs. N is the number of particles, ϵ is the softening parameter, $\epsilon_0 = 0.003735$, M_{BH}/m is the ratio between the BH mass and a particle mass, and ϵ/b_{min} the ratio between the softening parameter and the minimal impact parameter.

N	ϵ/ϵ_0	M_{BH}/m	ϵ/b_{min}	$\ln \Lambda$
16K	0	8.5	0	3.8
16K	1	8.5	2.6	3.6
80K	0	42.3	0	6.6
80K	0.01	42.3	0.03	6.0
80K	0.1	42.3	0.3	5.3
80K	1	42.3	2.6	4.8
80K	2	42.3	5.3	3.5
80K	8	42.3	21.2	2.8
80K	16	42.3	42.4	1.8

Table 4. Overview of the treecode runs. Meaning of symbols is the same as in Table 3 above.

N	ϵ/ϵ_0	M_{BH}/m	ϵ/b_{min}	$\ln \Lambda$
80K	1	42.3	2.6	4.7
400K	1	211.3	2.6	5.0
2M	1	1056.5	2.6	4.9
80K	0.1	42.3	0.3	5.7
80K	2	42.3	5.3	4.1
80K	8	42.3	21.2	3.0
80K	16	42.3	42.4	2.0
80K	32	42.3	84.7	1.6
80K	1	84.5	1.3	5.4
80K	1	169.0	0.7	4.6
400K	1	422.6	1.3	4.6
400K	1	845.2	0.7	4.2

Table 5. Overview of the PM runs. N is the number of particles, n the number of grid cells per dimension, m the particle mass, l the intermediate grid cell size, N_c the average number of particles per cell, m_c the average mass of a cell, M_{BH}/m_c the ratio between the BH mass and the cell mass, and finally l/b_{min} the ratio between the cell size and the minimal impact parameter.

N	n	m [M_{\odot}]	l [pc]	N_c [$\frac{\#}{\text{cell}}$]	m_c [$\frac{M_{\odot}}{\text{cell}}$]	$\frac{M_{BH}}{m_c}$	$\frac{l}{b_{min}}$	$\ln \Lambda$
80K	16	1475	1.60	46.3	68287.0	0.9	114.3	n/a
80K	32	1475	0.69	3.6	5375.4	11.6	49.3	1.9
400K		295	0.69	18.2	5375.4	11.6	49.3	2.1
2M		59	0.69	91.1	5375.4	11.6	49.3	2.2
80K	64	1475	0.32	0.4	546.3	114.5	22.9	3.0
400K		295	0.32	1.9	546.3	114.5	22.9	3.4
2M		59	0.32	9.3	546.3	114.5	22.9	3.0
80K	128	1475	0.15	0.04	61.9	1011	10.7	2.8
400K		295	0.15	0.2	61.9	1011	10.7	3.7
2M		59	0.15	1.0	61.9	1011	10.7	3.8
2M	256	59	0.076	0.1	7.4	8483	5.4	4.1

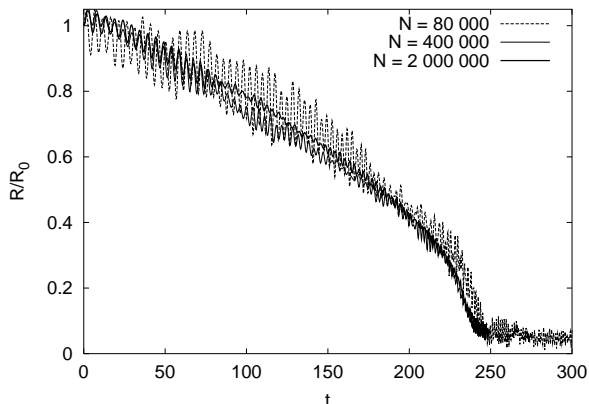


Figure 4. Time evolution of the radial distance of the black hole to the Galactic centre. The various curves (identified in the top right corner) present results obtained with the treecode. The X-axis is presented in N -body time units: one N -body time unit corresponds to about 0.031 Myr. The distance of the black hole to the Galactic centre (Y-axis) is given in terms of its initial distance. In these simulations is $\epsilon = 0.003735 \simeq 0.03$ pc and $M_{BH} = 0.000528$.

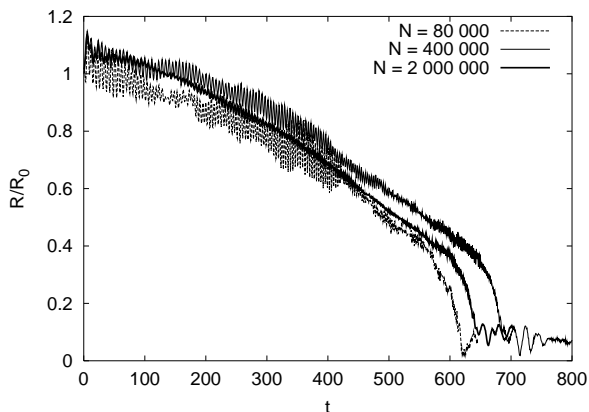


Figure 5. Same as Fig. 4 above, but for PM code simulations. The intermediate grid cell size is here $l = 0.69$ pc, and $M_{BH} = 0.000528$.

A resume of all the runs that we performed is reported in Table 3 for the PP code runs, Table 4 for the treecode runs, and finally Table 5 for the PM code runs. In all of our runs, the system remains in equilibrium during the whole BH infall, with no significant mass loss from stellar escapes, and a mass profile independent of time.

3.1 Dependence of $\ln \Lambda$ on N

In order to obtain a precise measure of $\ln \Lambda$, ideally one would run a direct N -body simulation with N of the order of the number of stars in the Galactic bulge, which amounts to $\sim 10^8$. Such high number makes a direct simulation unfeasible, and imposes the use of approximate methods instead. In order to evaluate the reliability of the approximate methods, we compared the PP code runs with the treecode runs. The PP code runs give a reliable picture of the system dynamics at low particle numbers, i.e. at high granularity. Using the treecode we can reach a number of particles much higher, even though about two orders of magnitude less than a realistic value yet. A comparison of the results from the two methods allows us to estimate the validity of the treecode runs, up to 2 mil-

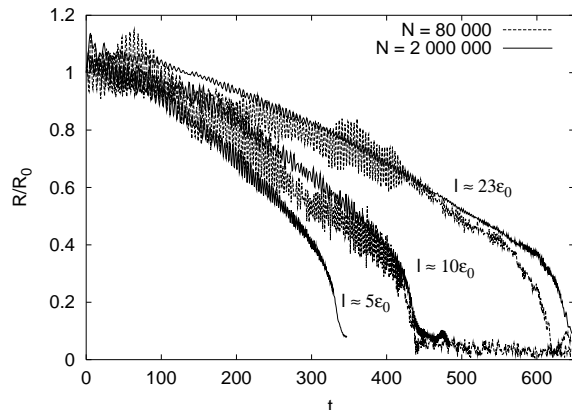


Figure 6. Black hole infall at various cell sizes, and large difference in N . Results here are from PM code simulations. The case $N = 80\,000$, $l \simeq 5\epsilon_0$ is not shown for readability reasons, since it would overlap with the $l \simeq 10\epsilon_0$ results.

lion particles. Then we can compare the treecode runs and the PM runs, in order to validate the results from the latter, which has the capability to simulate systems of about 100 million stars. In such a way we will eventually be able to study the infall of a BH into the Galactic centre in a simulation environment with a realistic value of N .

In Fig. 4 we show the evolution of the BH distance from the centre of mass of the system for three treecode simulations. N varies from 80 000 to 400 000 and 2 million, with $\epsilon = \epsilon_0 = 0.003735$, corresponding to about 0.03 pc. In Fig. 5 we present a similar figure from PM code simulations. Here is $N \in \{80\,000, 400\,000, 2\,000\,000\}$, with 32 cells per dimension, resulting in a cell size of about 0.69 pc.

Figs 4 and 5 show that increasing N results in a much smoother motion of the BH in its infall towards the centre of the Galaxy. The BH infall rate is not much affected by a change in N . Accordingly, the value of $\ln \Lambda$ for each of the two sets above is consistent, as values in Table 4 (first three rows) and Table 5 (rows with $l = 0.69$) show.

In order to study further the extent of the influence of N on the infall rate of the BH, and hence in $\ln \Lambda$, we compare in Fig. 6 results from PM code simulations with increasing grid refinement, and extreme difference in N . To quantify the grid resolution, we use the cell length at intermediate refinement, which is the cell length pertaining to the physical region where the BH evolves for most of its infall. We measure this length in units of $\epsilon_0 = 0.003735$, which makes the comparison with the softening parameter of the treecode easier. N has no remarkable influence on the infall rate, except for the case where the cell size is $l = 0.15$ pc $\simeq 5\epsilon_0$. In this case the simulation with $N = 80\,000$ (data not reported in the figure), shows an incorrect BH infall, comparable to the case $l = 0.32 \simeq 10\epsilon_0$. This can be explained by the fact that in the low l , low N case, the cells are so small, and the particles so few, that many cells in the PM grid are empty (see also the N_c column in table 5, which gives the average number of particles per cell). When $N_c \ll 1$, the density field is incorrect, with many grid points having a null value, because the corresponding cell is empty. In this condition, the gravity field computed by the PM code becomes unreliable, affecting the numerical results, as in the simulation with $N = 80\,000$ and $l \simeq 5\epsilon_0$.

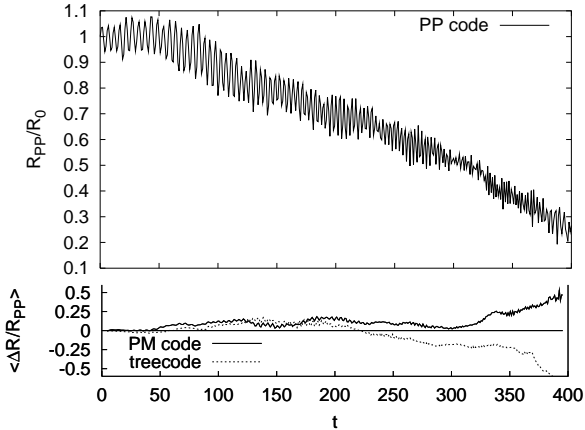


Figure 7. Top panel shows a black hole infall simulated by the PP code, with $N = 80\,000$, $M_{BH} = 0.000528$ and $\epsilon = 8\epsilon_0$. Bottom panel shows a comparison of the PP results with treecode and PM results. Parameter values are in all cases the same, except for the PM cell size, which is $l = 10\epsilon_0$. Plotted values are averages over 10 time units.

3.2 Comparison of the codes

In this section we compare the results obtained from the various codes, to check their consistency. The comparison of the PM results with the two other codes results is particularly critical, since the PM code computes forces using a different mathematical approach, i.e. a grid based force derivation vs a direct particle-particle computation for the PP code, or particle-multipole computation for the treecode. A consequence of this is a different parameter to tune the accuracy of the simulation, namely the cell size l for the PM code, and the softening length ϵ for the other two codes. We will study here how these two parameters influence the black hole infall.

In Fig. 7 we show the time evolution of the galactocentric BH distance R simulated by the PP code, accompanied by a plot of the time evolution of $\Delta R/R_{PP}$ for treecode and PM simulations, where $\Delta R = (R - R_{PP})$. The relative difference $\Delta R/R_{PP}$ remains small for a large fraction of the infall, and the final discrepancy is mostly due to the small values of the quantities at that point, which are likely to amplify relative differences. As the following figures also show, the BH infall is predicted with very good consistency among the codes.

In Fig. 8 selected treecode runs with $N = 80\,000$ and increasing ϵ are compared with the direct code runs having the same values of N and ϵ . At the same time, the figure shows how the infall time increases (and implicitly how $\ln \Lambda$ decreases), as ϵ increases. Fig. 8 and Table 6 show that the results from the treecode, the PP code, and the PM code are in good agreement. The agreement of the results from the three methods, and the scaling of $\ln \Lambda$ with ϵ , will be further studied quantitatively in Section 3.4.

In order to understand how the cell length l of the PM code and the softening parameter ϵ of the PP code and treecode relate with each other, we compare in Fig. 9 the results from the PM code and treecode simulations with 80 000 particles. The BH infall as shown in Fig. 9 depends on the value of l or ϵ . Remarkably, l and ϵ seem to play the same role not only qualitatively, but also quantitatively: in a PM run, a given value of l induces an infall which is very similar to the infall, in a treecode run, with ϵ assuming that same value. In Section 3.4 this relation will be studied further.

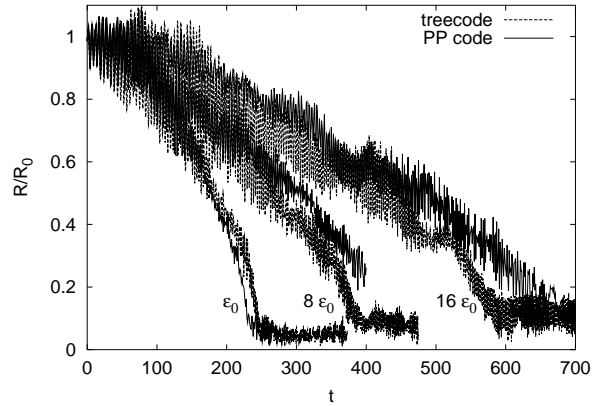


Figure 8. Comparison of results from the PP code with results from the treecode, at different values of ϵ . For all cases shown here is $N = 80\,000$ and $M_{BH} = 0.000528$. The PP simulation with $\epsilon = 8\epsilon_0$ has been already shown in Fig. 7.

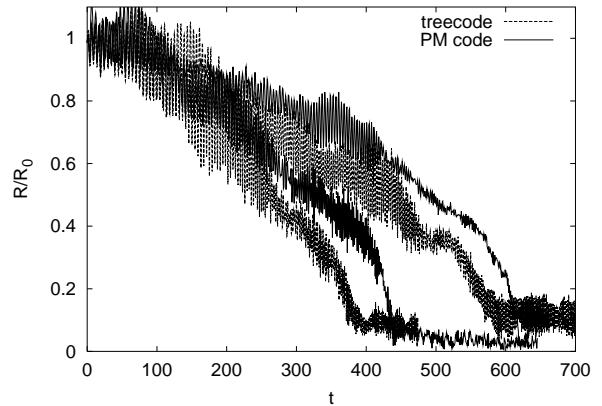


Figure 9. Comparison of PM results with treecode results. PM simulations have cell size l equal to resp. $10\epsilon_0$ and $23\epsilon_0$; softening parameters in the treecode runs are resp. $8\epsilon_0$ and $16\epsilon_0$. In all the above cases, is $N = 80\,000$ and $M_{BH} = 0.000528$.

3.3 The effect of softening/grid

The influence of the softening parameter on the BH dynamics has been studied by running a number of simulations with the three codes. In Table 6 we report the value of $\ln \Lambda$ obtained from our simulations. For the PP code and treecode simulations, we increase ϵ from 0 to $32\epsilon_0 = 0.1195 \simeq 0.96$ pc. For the PM code, we increase l from $2.5\epsilon_0$ to $23\epsilon_0$. In all cases is $M_{BH} = 0.528 \cdot 10^{-3} \simeq 62\,300 M_\odot$.

For the PP code and the treecode, we selected $N = 80\,000$ as a suitable value. The relaxation time is for this value of N $t_x \simeq 0.1N / \ln N \cdot R / v_{typ} \simeq 2000$, about one order of magnitude larger than the typical BH infall time, so that the system is collisionless, and we can confidently use the treecode to simulate it. With this choice for N , the BH mass is $M_{BH}/m \simeq 42.3$, (see Table 4). As a cross-check, we ran two PP runs with $N = 16\,000$ which, as expected, gave incorrect results (see Table 3). This is due to both a too small M_{BH}/m ratio, and a too short relaxation time ($t_x \simeq 400$ in this case). We did not increase ϵ above $\simeq 0.12$, since at this point ϵ is already much bigger than b_{min} (see Table 4), and the infall time is now close to t_x .

Table 6. $\ln \Lambda$ versus ϵ from PP code, treecode, and PM code runs. For the PP code and treecode runs is $N = 80\,000$. For the PM code runs is $N = 2$ million. The reference value for the accuracy parameter is $\epsilon_0 = 0.003735$.

ϵ/ϵ_0	PP code	treecode	l/ϵ_0	PM code
0	6.6			
0.01	6.0			
0.1	5.3	5.7		
1	4.8	4.7		
2	3.5	4.1	2.5	4.1
8	2.8	3.0	5	3.8
16	1.8	2.0	10	3.0
32		1.6	23	2.2

For the PM code simulations, we used $N = 2$ million in order to have enough particles to fill all the cells, even for the simulations with a small l . As Table 5 shows, for $l = 0.076\text{pc} \simeq 2.5\epsilon_0$ the average number of particles per cell is already $N_c = 0.1$. Since a PM simulation gives incorrect results for $N_c \ll 1$ (see also the discussion at the end of Section 3.1), we did not decrease l below 2.5.

The decrease of the value of $\ln \Lambda$ as ϵ or l increases is clear from Table 6. In the next sub-section we focus on the relation between Λ and ϵ , and provide a fitting formula for $\ln \Lambda(\epsilon)$. We use hereafter ϵ to refer either to the softening length of the PP and treecode, or to the cell size of the PM code. As shown on Fig. 9 and discussed above, these two parameters play the same role even quantitatively in affecting $\ln \Lambda$. In this respect, we refer to ϵ as a generic accuracy parameter.

3.4 Determination of $\ln \Lambda$

We will study here the relation between ϵ and $\ln \Lambda$. As just said above, in this context ϵ will be used as the accuracy parameter, and it will refer to either the softening length used in the PP and treecode, or to the cell size in the PM code.

A mathematical expression for the relation between ϵ and $\ln \Lambda$ can be found by considering how softening affects two body scattering. The role of ϵ is to prevent too close stellar encounters. In this respect, the effect of introducing a softening length is to increase the minimal impact parameter. Hence, we can define an effective impact parameter $b_{eff} = b_{min} + \epsilon$, and we modify equation (3) to become:

$$\ln \Lambda = \ln \frac{b_{max}}{b_{eff}} = \ln \frac{b_{max}}{b_{min} + \epsilon}. \quad (10)$$

We will now fit this equation with the values reported in Table 6. In order to perform the fit, we change equation (10) in a more suitable form, as follows:

$$\ln \Lambda = \ln b_{max} - \ln(b_{min} + \epsilon) = K - \ln(a + \epsilon). \quad (11)$$

We will refer to b_{max} and b_{min} as the theoretical values of the maximal and minimal impact parameters, as they can be obtained from equations (2) and (3), and K and a as the corresponding experimental values obtained with the fit.

The best fits for K and a with respect to simulation values are reported in Table 7 for all codes. Such fits have been performed with a fixed value for R_0 , i.e. the $R_0 = R_{hm}$. In fact, the not perfectly circular orbit of the BH results in an oscillatory behaviour for the BH galactocentric radius. In this case, having R_0 fixed could not be an appropriate choice for the fit. We checked whether having

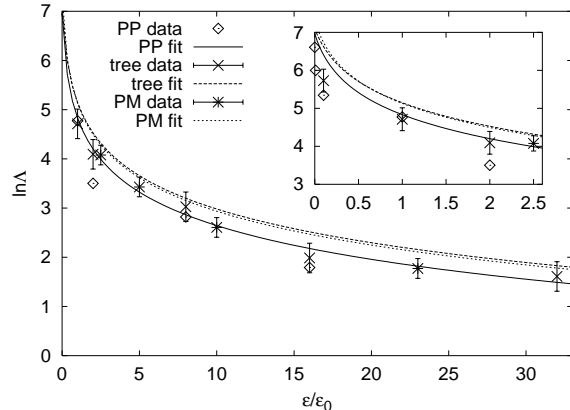


Figure 10. $\ln \Lambda$ vs ϵ , and best fit for $\ln \Lambda = K - \ln(a + \epsilon)$. Values for K and a are given in Table 7. The inset in the figure is a magnification of the low ϵ region. In all cases is $M_{BH} = 0.000528$. For the PP and treecode runs is $N = 80\,000$, for the PM code runs is $N = 2\,000\,000$. Error bars are omitted from the PP values to improve readability. For the same reason, $\ln \Lambda$ values for $\epsilon/\epsilon_0 < 1$ are shown only in the inset.

Table 7. Best values for the parameters K and a , and error on $\ln \Lambda$ for the fit of $\ln \Lambda = K - \ln(a + \epsilon)$.

	PP code	treecode	PM code
K	-0.94 ± 0.21	-0.64 ± 0.10	-0.59 ± 0.05
$a \cdot 10^{-3}$	0.80 ± 0.28	0.88 ± 0.20	0.74 ± 0.08
$\Delta(\ln \Lambda)$	0.6	0.3	0.2

R_0 as a free parameter in the fit leads to different results in $\ln \Lambda$. We obtained values for $\ln \Lambda$ within the error bars in Fig. 10, and values for R_0 within $R_{hm} \pm 0.05$. We can conclude that, although the galactocentric BH radius does not decrease smoothly, but in an oscillatory fashion, having R_0 fixed to the actual initial BH radius in the simulations leads to correct fits for the value of $\ln \Lambda$. With respect to the PM values, a further peculiarity is that when the BH enters the finest grid area, i.e. approximately at $R = 0.3$, the value of l decreases, because the BH enters the finest grid area (see Section 2.3 and Fig. 2). This causes b_{eff} to become smaller, increasing the value of $\ln \Lambda$. In fact, a fit of the PM data limited to values of $R > 0.3$ gives values of $\ln \Lambda$ systematically higher by $\simeq 0.3 \simeq 2\Delta(\ln \Lambda)$.

From the PP code value of K in Table 7 we obtain for b_{max} the experimental value $b_{max}^E = e^K \simeq 0.39$. This value is quite smaller than what one would expect. Since b_{max} has the meaning of the maximal impact parameter, a natural choice is to assign it a value of the order of the system size, which in our case would result in $b_{max} = 2$. The maximal radius for dynamical friction in our system is then about one quarter of what it is customarily assumed. PM and treecode values are slightly higher, but still quite smaller than $b_{max} = 2$. Also a is smaller than the theoretical value $b_{min} = G \cdot (M_{BH} + m)/v_{typ}^2 = 1.41 \cdot 10^{-3}$, by a factor 3. The a value for all codes is perfectly consistent.

An explanation for the discrepancy between the values of b_{max} and b_{max}^E is that the BH, while moving to the Galactic centre, is off-centre with respect to the density peak (in fact the BH is spiralling towards it). With respect to the BH position, the density distribution is then asymmetric. This density peak has clearly a greater influence on the BH dynamics, contributing more than the other regions of the system to the dynamical friction on the BH.

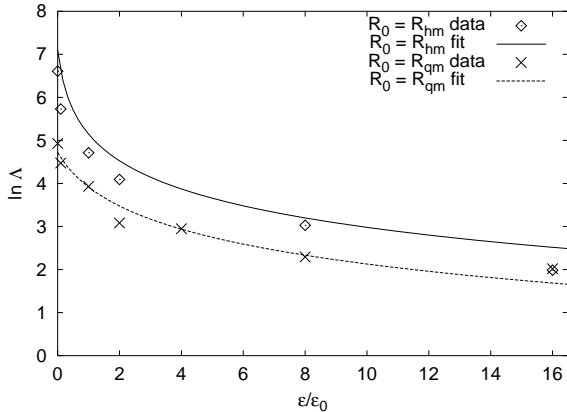


Figure 11. Comparison of $\ln \Lambda$ vs ϵ at different initial galactocentric BH radii. The smaller values of $\ln \Lambda$ for the cases with $R_0 = R_{qm}$ indicate that b_{max} is influenced by the galactocentric BH radius.

This leads to a value of b_{max} affected by the galactocentric BH radius. This approach is studied in detail by Hashimoto et al. (2002), who propose the galactocentric radius as a value for b_{max} in the context of the spiralsation of satellite galaxies.

In our simulations, the galactocentric radius varies from $R \simeq 0.9$ at the beginning of a simulation, to $R \simeq 0$ at the end of it. The value of b_{max}^E that we find is within this range, and it can be interpreted as an order 0 estimate of a maximal impact parameter that depends on the galactocentric BH radius.

In order to explore this aspect further, we simulated the infall of the same BH, starting at the quarter mass radius $R_{qm} \simeq 0.43$, for ϵ ranging from 0 to $16\epsilon_0$. What we expect is a smaller value of b_{max}^E , hence smaller values of $\ln \Lambda$. All simulations are performed with the treecode, except for the $\epsilon = 0$ case, which is simulated with the PP code. Our results are in Fig. 11. We can see there how smaller are the values of $\ln \Lambda$ for the cases when the BH starts at the quarter mass radius. A fit on these data gives $K \simeq -1.1$, which implies $b_{max}^E \simeq 0.33$, which is smaller than the value of b_{max}^E obtained for the BH starting from the half mass radius. Our findings support the argument of Hashimoto et al. (2002).

3.5 Variable black hole mass

We also studied the effect of a variable BH mass on the value of $\ln \Lambda$. We simulated, using the treecode, the infall of a BH of mass two times and four times larger than the default mass $M_0 = 0.528 \cdot 10^{-3} \simeq 0.62 \cdot 10^5 M_\odot$. We studied this infall in both the 80 000 particles configuration, and the 400 000 particles configuration. In all cases, we used our standard value for ϵ , i.e. $\epsilon_0 = 0.003735$. In Fig. 12 the distance r of the BH from the centre of mass of the system is shown for all the cases mentioned above, together with the $M_{BH} = M_0$ cases. From equation (11) and Table 7, the appropriate value for $\ln \Lambda$ in the above cases is:

$$\ln \Lambda = K - \ln(a + \epsilon_0) \pm \Delta = -0.64 - \ln(0.00088 + 0.003735) \pm 0.3 \simeq 4.7 \pm 0.3.$$

We also show in Fig. 12 the analytic curve $r(t)$, as given by equation (5), with $\ln \Lambda = 4.7$. An error bar gives, for each analytical curve, the spread corresponding to a variance $\Delta(\ln \Lambda) = 0.3$.

The results shown in Fig. 12 are consistent with the hypothesis that a variation in the BH mass has a little effect in the value of $\ln \Lambda$. In fact, $\ln \Lambda$ shows a logarithmic dependence on M_{BH}

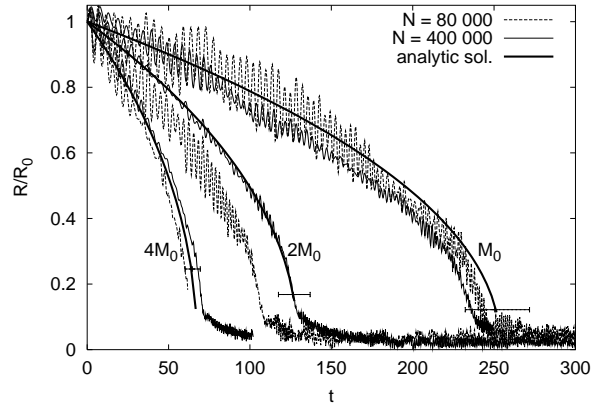


Figure 12. Black hole infall for different values of the BH mass, and different values of N . Simulations are performed with the treecode. Simulation results are compared with the analytic solution, equation (5), with $\ln \Lambda$ obtained from equation (11) and Table 7. The error bars at the bottom of the analytic curves correspond to a variance $\Delta(\ln \Lambda) = \pm 0.3$.

through the parameter b_{min} , which depends linearly on M_{BH} (see equations (2) and (3)). Assuming that also the experimental value a depends linearly on M_{BH} , we obtain $\ln \Lambda \simeq 4.6 \pm 0.3$, and $\ln \Lambda \simeq 4.4 \pm 0.3$ respectively for the $2 M_{BH}$ case and the $4 M_{BH}$ case. This results in a small displacement towards the right of the corresponding analytic curves in Fig. 12, which does not affect the conclusions that can be drawn from the figure. The theoretical curve fits very well with the $M = 2 M_0$, $N = 400 000$ case. The other simulation curves are within, or very close to, the error in $r(t)$ associated to the error in $\ln \Lambda$. We can conclude that a variation in the mass of the infalling object has little influence in the value of $\ln \Lambda$, which is important in view of extending this work to the case of the infall of a star cluster.

The fitting formula for $\ln \Lambda$ vs ϵ was obtained from simulations with $M_{BH} = M_0$. This formula predicts $\ln \Lambda$ for the cases with $M_{BH} > M_0$ with a very good accuracy, showing that it can be applied in a more general context, in order to forecast the value of the Coulomb logarithm.

Fig. 12 also shows a dumping in the BH infall at very small values of R , especially for the $N = 400 000$ case. This effect, introduced in Section 2.5, is clearer in the $N = 400 000$ case, since the particle density is higher in this case, compared to the $N = 80 000$ case.

3.6 Comparison with related work

Milosavljević & Merritt (2001) study the dynamical evolution of two black holes, each one at the centre of a power law cusped galaxy core. They simulate the merging of the two galaxies, which results in the two black holes forming a hard binary at the centre of the merged galaxy. In Section 3 of their paper they discuss the value of $\ln \Lambda$ in their simulations. They measure the decay rate of the two black holes, and compare this value with theoretical estimates. When they compare their experimental decay rate with an estimate for the case of the infall of an isolated black hole, they find a theoretical estimate about 6 times lower than the measured value, under the assumption that $\ln \Lambda \simeq 1.6$. If the value of $\ln \Lambda$ is not theoretically pre-determined, and is instead obtained from the decay rate equation, the result is $\ln \Lambda \simeq 10$. Similarly, they compare the experimental value with an estimate for the case of two mu-

tually spiralling spherical distributions of matter. In this case they assume $\ln \Lambda \simeq 1.0$, and obtain an estimate for the decay rate about a factor of 2 lower than the observed value. Determining $\ln \Lambda$ from the measurement would give in this case $\ln \Lambda \simeq 1.87$. The values of $\ln \Lambda$ that we find are between the two values above.

The value for $\ln \Lambda \simeq 1$ that they assume in their theoretical estimates, comes from a derivation that they present in appendix A of the same work. This derivation is based on results of Maoz (1993). Under the assumption that the stellar density obeys a power law centered on the BH position:

$$\rho(r) = \rho_0 \left(\frac{r}{b_{min}} \right)^{-\alpha}, \quad (12)$$

they obtain $\Lambda \simeq 1/\alpha \simeq 1$, which actually implies $b_{max} \simeq b_{min}$, whereas it is customary to consider $b_{max} \gg b_{min}$.

Their assumption in fact is valid only when the BH is close to the centre of the power law distribution. In their context this is true when: 1) the separation between the two BHs is much larger than the half mass radius of the two galaxies. In this case each BH is at the centre of his galaxy, and at the same time his motion is not yet heavily perturbed by the other galaxy. 2) the BH binary has hardened, and occupies the centre of the merged galaxy.

During the transient phase, when the two BHs have not yet formed a binary, the density distribution that affects the motion of the BHs is double-cusped, with a BH in each of the two cusps. This is substantially different from the density distribution modelled by equation (12).

This qualitative argument would make the density distribution in equation (12) inapplicable during the transient phase, and could explain why Milosavljević & Merritt (2001) find a higher than expected value of $\ln \Lambda$ in the transient. The analytical evaluation of $\ln \Lambda$ according to the technique used by them is by no means trivial, when symmetry arguments cannot be straightforwardly applied. We will address this issue in future developments of the present work.

4 APPLICATIONS TO STAR CLUSTERS

Recent observations of the Galactic Centre have revealed a population of very young clusters with ages less than 10 Myr. The presence of such stars inside the inner pc of the Galaxy is puzzling, as the strong tidal field in the Galactic centre easily prevents star formation. The origin of these stars is therefore vividly debated (Gerhard 2001; McMillan & Portegies Zwart 2002; Kim & Morris 2002). Morris (1993) proposed that a star cluster at some distance from the Galactic centre could spiral-in due to dynamical friction (see also Gerhard (2001)). The efficiency of dynamical friction depends sensitively on the actual value of the Coulomb logarithm $\ln \Lambda$.

4.1 Sinking of massive black holes in the Galactic centre

We performed N -body simulations for a large range of conditions. In Section 3.1 we varied the number of particles, in Section 3.3 we varied the size of the object, and in Section 3.5 we varied its mass. With direct N -body simulations we measured the actual value of the Coulomb logarithm $\ln \Lambda$. We study the behaviour of $\ln \Lambda$ for various types of N -body solvers and particle numbers. We also study the behaviour of $\ln \Lambda$ as a function of the softening length ϵ . Only the direct N -body code can perform a true measurement of the Coulomb logarithm, because it is able to resolve even the

smallest length scales and time scales. This, however, makes the direct code very slow and, even using the very fast GRAPE-6 special purpose device, we are able to perform simulations with only 10^5 particles. This is a small number compared to the actual number of stars in the Galactic centre. With approximate methods (treecode and particle-mesh) we are able to increase the number of particles up to 2 million. The cost of this is a lower accuracy in calculating stellar motion below a typical length scale ϵ . We studied how this length scale influences $\ln \Lambda$, by affecting the value of the minimal impact parameter.

4.2 Young dense clusters in the Galactic centre

The study of the dependence of $\ln \Lambda$ on ϵ described above is also of astronomical interest, because ϵ can be interpreted as the typical length of a finite size infalling object. Based on this, our analysis of the dependence of $\ln \Lambda$ on ϵ can be seen as a first approach to the study of the infall of a star cluster of typical size ϵ toward the Galactic centre. We found (see Fig. 10) that the value of $\ln \Lambda$ decreases quite rapidly as ϵ increases, with the logarithm argument $\Lambda \propto 1/\epsilon$. The typical size of the compact young clusters observed in the Galactic bulge is $\simeq 0.3$ pc (Figer et al. 1999), which corresponds to $\epsilon \simeq 10\epsilon_0$. With this value of ϵ , from equation (11) and Table 7, we obtain $\ln \Lambda \simeq 2.9$, about 60% less than the value for a point mass. The infall time is roughly doubled. For our choice of object mass, $M \simeq 62\,300 M_\odot$, and initial galactocentric radius, $R_0 \simeq 7$ pc, we have an infall time that increases from $\simeq 6$ Myr for the point mass, to $\simeq 12.5$ Myr for an object of typical size $\simeq 10\epsilon_0 \simeq 0.3$ pc.

We also studied the uncertainty associated with the maximal impact parameter b_{max} . We found that for an infall to the Galactic centre, the infalling object is mostly influenced by the density peak at the Galactic centre itself. A good choice for b_{max} is then $b_{max} \simeq \beta R_0$, where R_0 is the initial galactocentric radius, and $\beta \simeq 0.5$.

5 CONCLUSIONS

We simulated the evolution of a massive particle in a sea of lighter particles in a self gravitating system. The main goal of this work is to obtain an accurate value of the Coulomb logarithm ($\ln \Lambda$). This helps us to understand the dynamics of the Galactic bulge and the rate at which intermediate mass black holes sink to the Galactic centre. We also study the effect of the finite size of the inspiraling object.

We ran both N -body particle-particle (PP) simulations, softened treecode simulations, and particle-mesh (PM) simulations. The comparative simulations are performed for 80 000 particles, and all result in the same value of $\ln \Lambda$. For a point particle near the Galactic centre we find $\ln \Lambda = 6.6 \pm 0.6$. In addition we measure the change in the Coulomb logarithm with respect to the softening parameter ϵ , which reveals $\Lambda \propto 1/\epsilon$. We argue that ϵ can be interpreted as the typical length of a finite size object, such as a star cluster, so that $\ln \Lambda$ as a function of ϵ can be seen as a first approximation of the dependence of the Coulomb logarithm on the size of an infalling star cluster.

We also observed a value of the maximal impact parameter b_{max} different from the customarily assumed value, which is proportional to the system size. We found that our results are more consistent to a value of b_{max} linearly dependent on the BH galactocentric radius, which is in agreement with Hashimoto et al. (2002).

We performed simulations with up to 2 million particles using

a treecode. The obtained value of $\ln \Lambda$ does not depend on the number of particles. Apparently, 80 000 particles is already enough to eliminate any granularity for our choice of initial conditions. The results of the treecode, at the low N -limit, are in excellent agreement with the PP simulations, and we find the same scaling with respect to ϵ . Increasing the black hole mass reduces the time scale for spiral-in as was expected from theory (see McMillan & Portegies Zwart 2002).

Finally we compared the results of our PP and treecode simulations with a particle mesh (PM) method. We compared the methods for N up to 2 million. The results of our PP, treecode, and PM calculations are in good agreement. The cell size in the PM model is directly comparable to the softening length ϵ in the PP and tree methods.

ACKNOWLEDGEMENTS

We thank Douglas Hoggie, Piet Hut, Jun Makino, and Steve McMillan for stimulating discussions. We acknowledge KNAW under grant 95-BTN-15, NWO under Spinoza grant 08-0, NOVA under grant V-37, DFG-grant FE564/1-1, EC through grant HPRI-1999-CT-00026. SPZ is a KNAW fellow.

REFERENCES

- Aarseth S. J., 1963, *MNRAS*, 126, 223
 Aarseth S. J., 1972, in Lecar M., ed., *The Gravitational N -body Problem* Reidel, Dordrecht, p. 373
 Aarseth S. J., 1985, in Brackbill J., Cohen B., eds, *Multiple Time Scales* Academic Press, Orlando, p. 378
 Aarseth S. J., 1999, *PASP*, 111, 1333
 Athanassoula E., Fady E., Lambert J.-C., Bosma A., 2000, *MNRAS*, 314, 475
 Barnes J. E., Hut P., 1986, *Nature*, 324, 446
 Binney J., Tremaine S., 1987, *Galactic Dynamics*. Princeton University Press, Princeton, New Jersey
 Chandrasekhar S., 1943, *ApJ*, 97, 255
 Cionco R., Brunini A., 2002, *MNRAS*, 334, 77
 Cora S. A., Muzzio J. C., Vergne M. M., 1997, *MNRAS*, 289, 253
 Fellhauer M., Kroupa P., Baumgardt H., Bien R., Boily C., Spurzem R., Wassmer N., 2000, *NewA*, 5, 305
 Figer D. F., Kim S. S., Morris M., Serabyn E., Rich R. M., McLean I. S., 1999, *ApJ*, 525, 750
 Gerhard O., 2001, *ApJ*, 546, L39
 Goldreich P., Tremaine S., 1980, *ApJ*, 241, 425
 Hashimoto Y., Funato Y., Makino J., 2002, *ApJ*, accepted
 Hoggie D., Mathieu R., 1985, in McMillan S. L. W., Hut P., eds, *The Use of Supercomputers in Stellar Dynamics*. Springer Verlag, Berlin, pp 233–235
 Hockney R. W., Eastwood J. W., 1988, *Computer Simulation Using Particles*. IOP Publishing Ltd, Bristol, England
 Kim S. S., Morris M., 2002, in preparation
 Krabbe A., Genzel R., Eckart A., Najarro F., Lutz D., Cameron M., Kroker H., Tacconi-Garman L. E., Thatte N., Weitzel L., Drapatz S., Geballe T., Sternberg A., Kudritzki R., 1995, *ApJ*, 447, L95
 Kustaanheimo P., Stiefel E., 1965, *Journal für die Reine und Angewandte Mathematik*, 218, 204
 McMillan S. L. W., 1986, in McMillan S. L. W., Hut P., eds, *The Use of Supercomputers in Stellar Dynamics* Springer Verlag, Berlin, p. 156
 McMillan S. L. W., Portegies Zwart S. F., 2002, submitted to *ApJ*
 Makino J., 1991, *PASJ*, 43, 621
 Makino J., 1997, *ApJ*, 478, 58
 Makino J., Aarseth S. J., 1992, *PASJ*, 44, 141
 Makino J., Fukushige T., Namura K., 2002, in preparation
 Maoz E., 1993, *MNRAS*, 263, 75
 Message Passing Interface Forum 1997, *MPI-2: Extensions to the Message-Passing Interface*. University of Tennessee, Knoxville, Tennessee
 Mezger P., Zylka R., Philipp S., Launhardt R., 1999, *A&A*, 348, 457
 Mikkola S., Aarseth S. J., 1990, *Celestial Mechanics and Dynamical Astronomy*, 47, 375
 Milosavljević M., Merritt D., 2001, *ApJ*, 563, 34
 Morris M., 1993, *ApJ*, 408, 496
 Nagata T., Woodward C., Shure M., Kobayashi N., 1995, *AJ*, 109, 1676
 Nagata T., Woodward C., Shure M., Pipher J., Okuda H., 1990, *ApJ*, 351, 83
 Okuda H., Shibai H., Nakagawa T., Matsuhara H., Kobayashi Y., Kaifu N., Nagata T., Gatley I., Geballe T., 1990, *ApJ*, 351, 89
 Portegies Zwart S. F., McMillan S. L. W., Hut P., Makino J., 2001, *MNRAS*, 321, 199
 Portegies Zwart S. F., Makino J., McMillan S. L. W., Hut P., 1999, *A&A*, 348, 117
 Salmon J. K., Warren M. S., 1994, *Journal of Computational Physics*, 111, 136
 Springel V., Yoshida N., White S. D. M., 2001, *NewA*, 6, 79
 Tamblyn P., Rieke G., 1993, *ApJ*, 414, 573
 van den Bosch F. C., Lewis G. F., Lake G., Stadel J., 1999, *ApJ*, 515, 50